The 4,4′-Dipyridyl Disulfide-Induced Formation of GroEL Monomers Is Cooperative and Leads to Increased Hydrophobic Exposure†

Markandeswar Panda, Alison L. Smoot, and Paul M. Horowitz*

Department of Biochemistry, University of Texas Health Science Center at San Antonio, San Antonio, Texas 78229-3900

Received April 23, 2001; Revised Manuscript Received July 2, 2001

ABSTRACT: The molecular chaperone, GroEL, is completely disassembled into monomers by the addition of 4,4′-dipyridyl disulfide. The dissociation leads to monomers in a kinetically controlled process. The additions of functional ligands of GroEL such as Mg^{2+} or adenine nucleotides produced differences in the observed rates, but at the end of the kinetics, the dissociation was complete. In addition to the information obtained from native gels, the fluorescent probe bis-ANS was utilized to follow the monomer formation. The results demonstrate that the formation of monomers was associated with the exposure of hydrophobic surfaces. This assessment was possible without the use of added chaotropes, such as urea, to dissociate GroEL. Dissociation kinetics were also followed by light scattering. The kinetics of dissociation of the 14mer are cooperative with respect to the concentration of 4,4′-DPDS. Thermodynamic parameters for the kinetic process gave a free energy of activation ($\Delta G^{\ddagger}$) of 19.3 ± 1.2 kcal mol^{-1}, which was decomposed to an enthalpy of activation ($\Delta H^{\ddagger}$) of 19.30 ± 1.2 kcal mol^{-1} and an entropy of activation ($\Delta S^{\ddagger}$) of −8.2 ± 3.9 cal mol^{-1} K^{-1}. We conclude that the dissociation of GroEL observed in this investigation is an enthalpy-controlled process.

Molecular chaperones assist protein folding in the cell by binding non-native proteins. GroEL, a molecular chaperone of *Escherichia coli*, is composed of 14 identical 57 kDa subunits arranged in two heptameric rings stacked back to back (*1*). The X-ray crystal structure shows that each of these subunits is composed of three domains: apical, intermediate, and equatorial (*1*−*3*). Crystal structures of GroEL fully complexed with 14 ATPγS[1] molecules (*2*) and the GroEL−GroES−$(ADP)_7$ complex (*4*) are also available. The apical domain (residues 197−376) forms the opening to the central channel of the cylindrical oligomer (*1*, *4*). It is also the binding site for peptides and GroES (*5*, *6*). The intermediate domain (residues 134−190 and 377−408) is a hinge region and plays a role in allosteric communication between the apical and equatorial domains (*1*, *4*, *7*). The highly helical equatorial domain makes up most of the intraring contacts and all of the interring contacts (residues 6−133 and 409−523), and provides the nucleotide-binding site (*2*−*4*, *7*). Each oligomeric ring forms a cylindrical cavity, which can vary from 6 to 13 nm depending upon the binding of divalent cations and nucleotides (*3*, *8*). The carboxylate oxygen of residue Asp389 is directly involved in Mg^{2+} coordination (*4*). The substrate protein becomes sequestered in the cavity for correct refolding and is prevented from aggregating and misfolding (*9*−*11*).

Another component of the system is the cochaperonin, GroES. GroES is composed of seven identical 10 kDa subunits and can bind to either end of the GroEL oligomer (*12*). In addition to GroES binding, ATP, K^+, and Mg^{2+} are also necessary for complete GroEL function (*10*, *13*−*16*). The binding of Mg^{2+}, ATP, and substrate polypeptide induces conformational changes in GroEL (*17*−*19*). ATP binds with both intraring positive cooperativity and interring negative cooperativity, and it serves as an energy source for the movements of GroEL subunits (*20*, *21*).

Hydrophobic interactions are considered to be involved in binding target proteins (*22*). The demonstration of hydrophobic exposure on GroEL monomers has been mostly from the studies involving the dissociation of the GroEL oligomer at subdenaturing concentrations of urea (*23*). The presence of chaotropes can have additional effects on the conformations of the released, potentially flexible subunits. Upon removal of urea by dialysis, the monomers reassociate to some extent and undergo conformational changes. This makes the process unsuitable for kinetic investigations (*24*). A single-point mutation K4E in the equatorial domain of GroEL results in permanent monomers (*25*). High hydrostatic pressure induces the formation of GroEL monomers, which do not readily reassociate to oligomers ($t_{1/2} \cong 150$ h) (*26*).

Each of the GroEL subunits contains three cysteines. Cys458 and Cys519 are located in the equatorial domain, and Cys138 is located in the intermediate domain. Formation of monomers following labeling with fluorescein-5-maleimide at Cys458 has been reported (*27*). Such labeled GroEL was able to bind unfolded rhodanese, but was unable to bind GroES. Recently, it has been reported that the monomer-

† This work was supported by National Institutes of Health Grant GM25177 and Robert A. Welch Foundation Grant AQ723 (to P.M.H.).

* To whom correspondence should be addressed: Department of Biochemistry, University of Texas Health Science Center at San Antonio, Mail Code 7760, 7703 Floyd Curl Dr., San Antonio, TX 78229-3900. Phone: (210) 567-3737. Fax: (210) 567-6595. E-mail: Horowitz@biochem.uthscsa.edu.

[1] Abbreviations: 4,4′-DPDS, 4,4′-dipyridyl disulfide; bis-ANS, 4,4′-dianilino(1,1′-dinaphthyl-5,5′-disulfonic acid, dipotassium salt); DTT, dithiothreitol; EtOH, ethanol; PAGE, polyacrylamide gel electrophoresis; EDTA, ethylenediaminetetraacetic acid; ATP, adenosine 5′-triphosphate; ADP, adenosine 5′-diphosphate; AMP, adenosine 5′-monophosphate; AMP-PNP, adenosine 5′-(β,γ-imido)triphosphate; ATPγS, adenosine 5′-*O*-(3-thiotriphosphate).

10.1021/bi010831x CCC: $20.00
Published on Web 08/03/2001

ization of GroEL can proceed through the formation of a mixed disulfide with Cys458 at high concentrations (142-fold over cysteine residues) of 4,4′-dithiodipyridine (4,4′-DPDS) (*28*) in the absence of chaotropes. The authors proposed a dissassembly scheme based on the results of this reaction with mutant GroELs and gel analysis of the products. However, no kinetic or mechanistic aspects were investigated. We have investigated some details of the effects of functional ligands of GroEL using 4,4′-DPDS-induced dissociation, since it has the potential of generating monomers more conveniently than the commonly available methods such as urea (*29*, *30*), guanidine hydrochloride (*30*), or pressure dissociation (*26*, *31*). The kinetics of formation of the GroEL monomers were followed in the presence of Mg^{2+} and nucleotides. Our study also allowed the estimation of the overall kinetic barrier of the dissociation process.

MATERIALS AND METHODS

Reagents and Proteins. 4,4′-Dianilino-1,1′-binaphthyl-5,5′-disulfonic acid, dipotassium salt (bis-ANS), was purchased from Molecular Probes, Inc. (Eugene, OR). 4,4′-Dipyridyl disulfide (4,4′-DPDS or aldrithiol-4) was purchased from Sigma (St. Louis, MO). All other reagents were analytical grade. GroEL (*32*) was expressed in *E. coli* and purified as described previously.

Monomerization of GroEL. GroEL was diluted to a concentration of 1.25 μM in various buffers. DPDS was diluted in various buffers from a stock solution of 0.52 M in 100% EtOH to 15 mM DPDS in <1% EtOH. Five microliters of 1.25 μM GroEL was mixed with 2.5 μL of 15 mM DPDS (142-fold excess over cysteine residues contained within GroEL) and the mixture allowed to incubate over various periods of time. The amounts of monomers that formed were analyzed using native polyacrylamide gel electrophoresis on 4% continuous, 5% discontinuous, or 6.5% discontinuous gels as needed for a particular experiment. All gels were stained with Coomassie Blue G stain to enhance the sensitivity of the bands. GroEL monomers used as controls were formed by incubation in 2.5 M urea (*34*), or using high pressure (*26*). The band intensities were scanned using the program Scion Image for Windows (IBM personal computer), based on NIH Image (for Macintosh). The Windows version was downloaded from Scion Corp. (Frederick, MD) (*35*).

Isolation of 4,4′-DPDS-Formed Monomers. The products from the 4,4′-DPDS monomerization reaction were passed over a P6-DG desalting column (Bio-Rad), pre-equilibrated in buffer with varying concentrations of 4,4′-DPDS. Samples were then allowed to incubate at room temperature over time.

Sedimentation Analysis. GroEL samples were subjected to sedimentation velocity analysis at 25 °C using a Beckman XL-A analytical ultracentrifuge with a rotor speed of 45 000 rpm in 10 mM sodium phosphate (pH 7.6). GroEL was diluted into 10 mM sodium phosphate buffer (pH 7.6). 4,4′-DPDS-formed monomer samples were incubated in either no 4,4′-DPDS or 35 μM 4,4′-DPDS (1:1 ratio of cysteine residues to 4,4′-DPDS). The sedimentation boundary was monitored at 230 nm (absorbance of the peptide bond) and 280 nm (absorbance of the aromatic side chains). The data were analyzed using the method of van Holde and Weischet (*36*) using the UltraScan ultracentrifuge data collection and analysis program (*37*). The partial specific volume was estimated from the amino acid sequence using the method of Sober (*38*).

Bis-ANS Fluorescence and Kinetics. All concentrations are final concentrations. All experiments were carried out at least twice, and the results were averaged. Bis-ANS was added at 5 μM to 0.83 μM GroEL in 10 mM sodium phosphate buffer (pH 7.6). Fluorescence scans were recorded at 25 °C using a Fluorolog-3 spectrofluorometer (ISA, Jobin Yvon-Spex, Edison, NJ) with an excitation wavelength of 395 nm. The slit widths were 2 and 5 nm for excitation and emission, respectively. For kinetic studies using fluorescence, the excitation was at 395 nm (slit, 2 nm) and emission was recorded at 495 nm (slit, 2 nm). The scattering kinetics were followed under identical conditions except that both excitation and emission wavelengths were set at 400 nm.

GroEL (0.83 μM) was incubated with bis-ANS (5 μM) in 10 mM sodium phosphate (Na_2HPO_4/NaH_2PO_4) buffer (pH 7.6, 1 mL volume) at 25 °C for 1 h prior to the addition of 4,4′-DPDS. After 15 min, the increase in bis-ANS fluorescence reached a plateau (data not shown). This solution also contained Mg^{2+} and/or nucleotides in experiments when needed, and was incubated for 1 h. In experiments where the temperature of the reaction mixture was varied, the samples were thermostated for at least 1 h to ensure thermal equilibration. Then 4,4′-DPDS was added (5 mM final 4,4′-DPDS concentration, 333-fold excess over cysteine residues), and either bis-ANS fluorescence or light scattering was followed as a function of time.

There was no self-dissociation of GroEL either in the absence or in the presence of bis-ANS before the addition of 4,4′-DPDS. This was confirmed by control experiments where both fluorescence and light scattering were monitored. The rates were evaluated by fitting the data to either a monoexponential (eq 1) or biexponential equation (eq 2):

$$Y = A_1 \exp(-k_1 t) + A_2 \quad (1)$$

$$Y = A_1 \exp(-k_1 t) + A_2 \exp(-k_2 t) + A_3 \quad (2)$$

The independent variable Y was the observed fluorescence or scattering intensity in counts per second (cps) after subtracting the fluorescence or scattering due to buffer. The pseudo-first-order rate constants k_1 and k_2 and parameters A_1, A_2, and A_3 were obtained from iterative nonlinear least-squares regression of the data using the Origin software program (MicroCal Software, Inc., Northampton, MA).

Thermodynamic Parameters. Thermodynamic parameters for the dissociation kinetics were calculated from the dependence of the observed rates on temperature. Transition state theory relates the individual rate constants to the difference in Gibbs free energy between the initial and transition state via eq 3 (*39*).

$$k_{obs} = (k_B T/h) \exp(-\Delta G^{\ddagger}/RT) \quad (3)$$

where k_{obs} is the observed rate constant for dissociation at any particular temperature (T in Kelvin), k_B is the Boltzmann constant (1.381×10^{-23} J K^{-1}), h is Planck's constant (6.626×10^{-34} J s), and R is the gas constant (1.987 cal mol^{-1} K^{-1}). The activation free energy is decomposed into its enthalpic and entropic components as shown in eq 4 (*39*).

$$\Delta G^{\ddagger} = \Delta H^{\ddagger} - T\Delta S^{\ddagger} \quad (4)$$

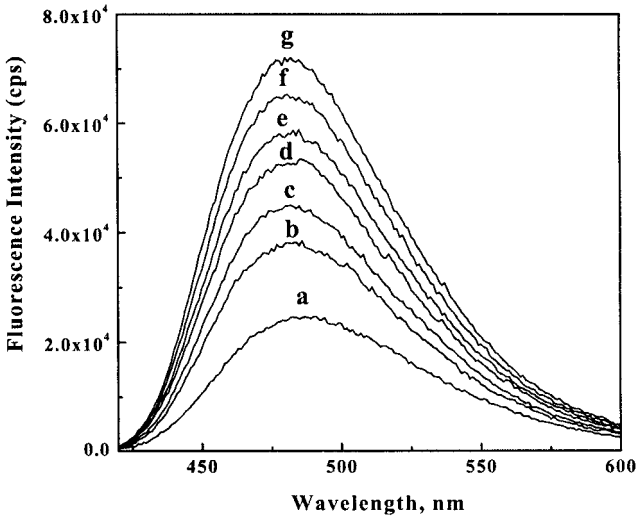

FIGURE 1: Emission spectra of bis-ANS binding to GroEL upon addition of 4,4′-DPDS as a function of time. Kinetic scans were recorded (see Materials and Methods) after adding 5 mM 4,4′-DPDS to a solution of 0.83 μM GroEL and 5 μM bis-ANS. The GroEL and bis-ANS solution was preincubated at 25 °C for 1 h before the addition of 4,4′-DPDS. The reaction conditions were as follows: 10 mM Na_2HPO_4/NaH_2PO_4, pH 7.6, and 25 °C. The excitation wavelength was 395 nm. The excitation and emission path lengths were 0.5 and 0.25 cm, respectively, and both slits were at 2 nm (band-pass). Scans a−g were recorded 0.5, 2.5, 5, 10, 15, 25, and 90 min after the addition of 4,4′-DPDS, respectively.

Combining eqs 3 and 4 leads to eq 5.

$$\ln(k_{obs}/T) = -(\Delta H^{\ddagger}/RT) + (\Delta S^{\ddagger}/R) + \ln(k_B T/h) \quad (5)$$

A plot of $\ln(k_{obs}/T)$ versus $1/T$ leads to a slope of $-(\Delta H^{\ddagger}/R)$ and an intercept of $23.76 + \Delta S^{\ddagger}/R$. The number 23.76 is the value of $\ln(k_B/h)$, since the required value for the transition state theory for $\ln(k_B T/h)$ at 298.16 K is 6.212×10^{12} s^{-1} (*40*). Errors in activation parameters were analyzed as discussed in the literature (*41*).

RESULTS

Bis-ANS Binding to Exposed Hydrophobic Surfaces of GroEL Induced by 4,4′-DPDS Binding. Emission scans of the fluorescence of bis-ANS bound to exposed hydrophobic sites as a function of time after addition of 4,4′-DPDS are shown in Figure 1. The available binding sites on the native GroEL 14mer were allowed to be occupied by the added bis-ANS for 1 h and scanned. After the addition of 4,4′-DPDS, there is a rapid decrease in intensity after which the intensity increases with time. This rapid decrease is not shown in the kinetic traces as it occurred in the first 30 s and was found to be an artifact of rapid mixing. In the first 2.5 min, there is a shift in the maximum from 486 to 480 nm (scans a and b, Figure 1), after which the maximum remains at ~480 nm until the completion of the dissociation of the oligomer. This suggests that the initial binding sites are less hydrophobic than the subsequent ones. This constant-wavelength maximum for bound bis-ANS suggests that the character of the environment of this probe bound to either the GroEL 14mer or the dissociated monomers has not changed, although the number of binding sites increased as more hydrophobic surfaces were exposed as dissociation proceeded. This observation is in agreement with an earlier report from our laboratory which demonstrated that the GroEL 14mer displays restricted hydrophobic surfaces, binding only one to two molecules of bis-ANS (*30*). Upon urea dissociation (2.5 M urea) into the assembly competent monomers (*23*), the level of bis-ANS binding increases (*30*).

Kinetics of GroEL Dissociation by the 4,4′-DPDS Reaction. The kinetics followed by monitoring fluorescence at 495 nm (see Materials and Methods) showed an increase in intensity over a period of 2−5 h until a plateau was reached. In all cases, i.e., in the absence or presence of Mg^{2+} and/or nucleotides, the kinetic traces monitored by fluorescence were biphasic. The fluorescence intensity at the plateau is similar to the bis-ANS fluorescence detected by its binding to GroEL in 2.5 M urea due to the increase in hydrophobic exposure of the monomeric GroEL (data not shown). To obtain additional information about the dissociation kinetics, we monitored the reaction using light scattering (see Materials and Methods), where the scattering intensity decreased with the progress of the reaction, indicating the formation of monomers. Typical biphasic kinetics followed by fluorescence (panel A) and scattering (panel B) techniques are shown in Figure 2. The kinetics in the presence and absence of 2 mM AMP-PNP in 10 mM Mg^{2+}, 0.12 M KCl, and 1 mM 4,4′-DPDS shown in Figure 3 confirm the observation from gel analysis reported by Bochkareva et al. (*28*). The reactions whose progress is depicted in Figure 3 have 10 mM NaP_i buffer at pH 7.6, which is used throughout our investigation. Identical kinetic traces and observed rates were obtained (data not shown) when the buffer described by Bochkareva et al. (*28*) was used [45 mM Tris (pH 7.6) and 0.15 mM EDTA].

There are many cases in which the kinetics were biphasic when followed by light scattering, especially at low concentrations (~1 mM) of 4,4′-DPDS in the presence of Mg^{2+} (Figure 3A), in the presence of 5 mM 4,4′-DPDS with Mg^{2+} and AMP-PNP (Figure 2B), and in other cases as shown in Table 1. In the absence of Mg^{2+} and nucleotides, the reactions were apparently monophasic and fit to eq 1 (Figure 2C). Dependences of the observed psuedo-first-order rates (k_{obs}) were studied by varying the concentration of 4,4′-DPDS from 0.5 to 17.5 mM at the fixed $GroEL_{14mer}$ concentration of 0.83 μM under identical reaction conditions (see Materials and Methods). The plot of k_{obs} versus 4,4′-DPDS concentration is shown in Figure 4. The plot did not tend to reach a plateau at higher reagent concentrations, and beyond the 4,4′-DPDS concentration maximum of 17.5 mM, there was visible precipitation of the protein. The dependence is cooperative with respect to the concentration of 4,4′-DPDS. This indicates that the initial interactions of 4,4′-DPDS with GroEL facilitate later ones.

Isolation of 4-DPDS-Formed GroEL Monomers and Sedimentation Velocity. To facilitate comparison of the monomers formed by 4,4′-DPDS with monomers formed using other methods (high pressure or urea), attempts were made to isolate the formed GroEL monomers free from 4,4′-DPDS using a 1 mL G-50 Sephadex spin column (Pharmacia, Piscataway, NJ). The yields of monomers recovered from these columns were extremely low, but enough material could be obtained for sedimentation analysis. This was most probably due to the increased hydrophobic exposure of the monomers, which would allow them adhere to the column material.

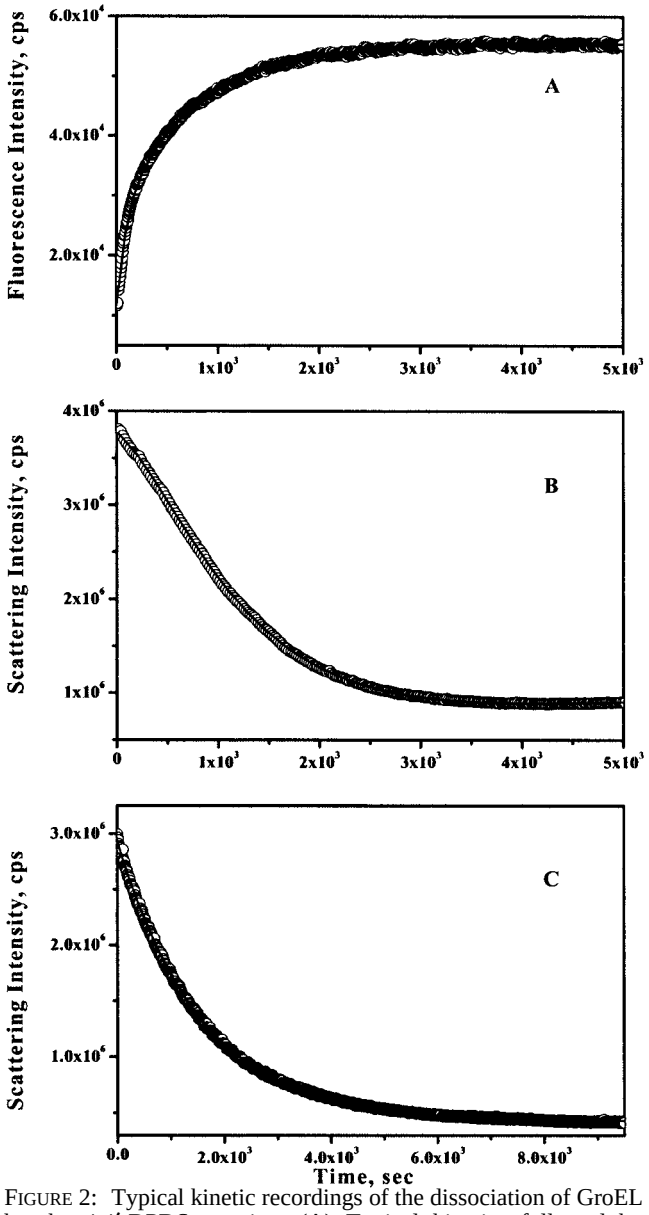

FIGURE 2: Typical kinetic recordings of the dissociation of GroEL by the 4,4′-DPDS reaction. (A) Typical kinetics followed by monitoring the binding of bis-ANS to the exposed hydrophobic surface on GroEL upon addition of 4,4′-DPDS. Kinetics were monitored by exciting the reaction sample at 395 nm and recording the emission at 495 nm. The reaction conditions were as follows: 0.83 μM GroEL 14mer, 5 μM bis-ANS, 5.0 mM 4,4′-DPDS, 10 mM Na_2HPO_4/NaH_2PO_4, pH 7.6, and 25 °C. The excitation and emission path lengths were 0.5 and 0.25 cm, respectively, and both slits were at 2 nm (band-pass). (B) Typical biphasic kinetics showing a lag phase followed by monitoring the scattering intensity of the reaction of GroEL (preincubated with bis-ANS) with 4,4′-DPDS. The reaction conditions were as follows: 0.83 μM GroEL 14mer, 5 μM bis-ANS, 5.0 mM 4,4′-DPDS, 10 mM Mg^{2+}, 1.0 mM AMP-PNP, 10 mM Na_2HPO_4/NaH_2PO_4, pH 7.6, and 25 °C. Scattering was monitored at 400 nm (excitation and emission wavelengths). The excitation and emission path lengths were 0.5 and 0.25 cm, respectively, and both slits were at 2 nm (band-pass). In panels A and B, the circles represent the data and the solid lines are the fits using the biexponential rate equation (eq 2). (C) Typical monophasic kinetics followed by monitoring the scattering intensity of the reaction of GroEL (preincubated with bis-ANS) with 4,4′-DPDS. The reaction conditions were as follows: 0.83 μM GroEL 14mer, 5 μM bis-ANS, 5.0 mM 4,4′-DPDS, 10 mM Na_2HPO_4/NaH_2PO_4, pH 7.6, and 25 °C. The circles represent the data, and the solid lines are the fits using the monoexponential rate equation (eq 1). The instrument settings are identical to those described for panel B.

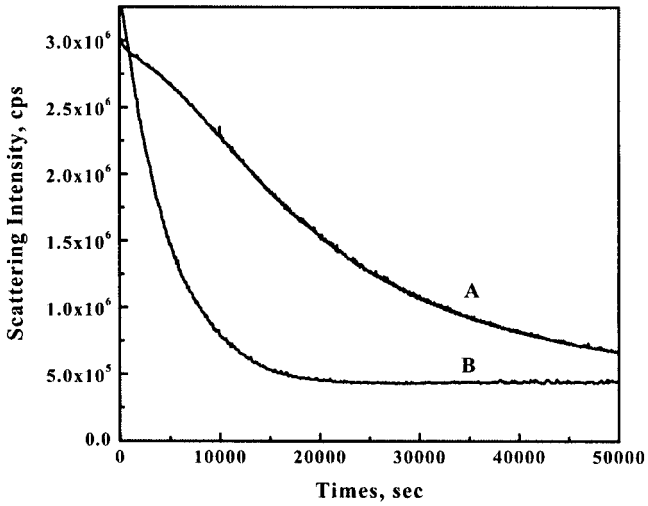

FIGURE 3: Effect of Mg^{2+}, AMP-PNP, and KCl on the kinetics of dissociation of GroEL by the 4,4′-DPDS reaction. The kinetic traces followed by light scattering (see Materials and Methods) are shown for comparing the effect on dissociation rates in the absence and presence of AMP-PNP. The reaction conditions were as follows: 0.83 μM GroEL 14mer, 1 mM 4,4′-DPDS, 0.12 M KCl, 10 mM Mg^{2+}, 10 mM Na_2HPO_4/NaH_2PO_4, pH 7.6, 25 °C, and (A) no AMP-PNP and (B) 2 mM AMP-PNP. These were identical to the reaction conditions used by Bochkareva et al. in their gel analyses studies (*28*).

To further investigate the state of the 4,4′-DPDS-formed monomers, sedimentation velocity data were collected on GroEL, the monomer formed by high-pressure treatment, and the 4,4′-DPDS-formed monomer with and without 3 mM 4,4′-DPDS (Figure 5). The occurrence of a vertical distribution of *S* values suggests a pure, single-component system. If more than 80% of the data is vertical, the system is considered to be homogeneous. Sedimentation velocity data for the GroEL oligomer revealed uniform $S_{20,w}$ values, denoting homogeneity, with an *S* value of approximately 21.75×10^{-13} s (only one data set, $A_{280} = 0.4$ shown for clarity) [Figure 5 (■)]. Data for the monomer formed by high pressure displayed a uniform $S_{20,w}$ value of 3.35×10^{-13} s (one data set, $A_{280} = 0.4$ shown for clarity) [Figure 5 (●)]. This observation is possible because the monomers formed by high pressure reassociate to oligomers very slowly ($t_{1/2} = 150$ h) (*26*). Data for the 4,4′-DPDS-formed monomers 2 h after removal of the excess reagent [Figure 5 (▲)] demonstrated a vertical section that correlates with ~40% homogeneity at an $S_{20,w}$ of approximately 2.5×10^{-13} s, with the remaining data spread from 2.5×10^{-13} to 22×10^{-13} s. This homogeneity was reduced to 20% [Figure 5 (△)] after 4 h. Taken together with the native gel data (data not shown), it is evident that the amount of monomer decreases over time and has a tendency to form higher-order aggregates. In contrast to this, 4,4′-DPDS monomers that have been passed over a column pre-equilibrated with buffer containing 35 μM 4,4′-DPDS (1:1 ratio of 4,4′-DPDS to cysteine residues) remain approximately 80% monomeric up to 6 h after isolation [Figure 5, right panel (◆ and ◇)]. Also, monomers stored in 35 μM 4,4′-DPDS were shown to remain in a monomeric state for up to 24 h (data not shown).

Native Gel Analysis of 4,4′-DPDS Monomerization of GroEL. The GroEL solutions at different times after the addition of 4,4′-DPDS were analyzed by native gel electrophoresis (see Materials and Methods). The results are shown

Table 1: Observed Pseudo-First-Order Rate Constants for the Dissociation of GroEL by 4,4′-DPDS in the Absence and Presence of 10 mM Mg^{2+} and/or 1 mM adenine nucleotides (0.83 μM GroEL, 5 mM 4,4′-DPDS, 10 mM NaH_2PO_4/Na_2HPO_4, pH 7.6, and 25 °C)[a]

addition	k_{1obs} (s^{-1})	k_{2obs} (s^{-1})
none	$(1.02 \pm 0.02) \times 10^{-2}$ (F) (34%)[b]	$(1.29 \pm 0.01) \times 10^{-3}$ (F) (66%)[c]
		$(6.50 \pm 0.02) \times 10^{-4}$ (S)[d]
0.12 M KCl with 0.2 M NaP_i	not observed	$(6.60 \pm 0.05) \times 10^{-4}$ (S)[d]
		$(9.70 \pm 0.09) \times 10^{-4}$ (S)[d]
Mg^{2+}	$(7.43 \pm 0.06) \times 10^{-3}$ (F) (26%)[b]	$(4.90 \pm 0.06) \times 10^{-4}$ (F) (74%)[c]
		$(5.60 \pm 1.10) \times 10^{-4}$ (S)[d]
Mg^{2+} with 0.12 M KCl		$(5.30 \pm 1.10) \times 10^{-4}$ (S)[d]
ATP	$(1.01 \pm 0.06) \times 10^{-2}$ (F) (33%)[b]	$(1.05 \pm 0.01) \times 10^{-3}$ (F) (67%)[c]
ADP	$(1.12 \pm 0.03) \times 10^{-2}$ (F) (35%)	$(1.10 \pm 0.01) \times 10^{-3}$ (F) (65%)[c]
AMP	not observed	$(1.14 \pm 0.01) \times 10^{-3}$ (F)
AMP-PNP	$(1.10 \pm 0.01) \times 10^{-2}$ (F) (34%)[b]	$(1.19 \pm 0.01) \times 10^{-3}$ (F) (66%)[c]
		$(7.50 \pm 0.03) \times 10^{-4}$ (S)
ATPγS	$(1.13 \pm 0.07) \times 10^{-2}$ (F) (60%)[b]	$(1.11 \pm 0.02) \times 10^{-3}$ (F) (40%)[c]
ATP with Mg^{2+}	$(1.08 \pm 0.10) \times 10^{-2}$ (F) (60%)[b]	$(7.20 \pm 0.20) \times 10^{-4}$ (F) (40%)[c]
	not observed (S)	$(9.90 \pm 0.06) \times 10^{-4}$ (S)[d]
(i) ADP with Mg^{2+}	$(1.68 \pm 0.11) \times 10^{-3}$ (S) (35%)[b]	$(7.60 \pm 0.30) \times 10^{-4}$ (S) (65%)[c]
(ii) no bis-ANS	$(1.08 \pm 0.21) \times 10^{-3}$ (S) (45%)[b]	$(8.90 \pm 1.50) \times 10^{-4}$ (S) (55%)[c]
AMP with Mg^{2+}	$(6.29 \pm 0.29) \times 10^{-3}$ (F) (33%)[b]	$(2.70 \pm 0.06) \times 10^{-4}$ (F) (67%)[c]
	not observed (S)	$(6.50 \pm 0.80) \times 10^{-4}$ (S)[d]
AMP-PNP with Mg^{2+}	$(1.00 \pm 0.02) \times 10^{-2}$ (F) (24%)[b]	$(1.28 \pm 0.04) \times 10^{-3}$ (F) (76%)[c]
AMP-PNP with Mg^{2+} and 0.12 M KCl	$(2.14 \pm 0.07) \times 10^{-3}$ (S) (32%)[b]	$(1.11 \pm 0.10) \times 10^{-3}$ (S) (68%)[c]
	$(2.22 \pm 0.16) \times 10^{-3}$ (S) (36%)[b]	$(1.38 \pm 0.05) \times 10^{-3}$ (S) (64%)[c]
ATPγS with Mg^{2+}	$(2.49 \pm 0.06) \times 10^{-3}$ (S) (32%)[b]	$(1.00 \pm 0.01) \times 10^{-3}$ (S) (68%)[c]
Mg^{2+} with 0.12 M KCl[e]	$(1.70 \pm 0.04) \times 10^{-4}$ (S) (26%)[b]	$(6.00 \pm 0.05) \times 10^{-5}$ (S) (74%)[c]
AMP-PNP with Mg^{2+} and 0.12 M KCl[e]	$(2.10 \pm 0.01) \times 10^{-4}$ (S)	not observed (S)

[a] F, fluorescence; S, scattering. [b] The values in parentheses are the relative magnitudes of the amplitudes of the fast phases in a reaction assuming the sum of the two phases equals 100%. The amplitudes were obtained from the fits of the kinetic data using eq 2. [c] The values in parentheses are the relative magnitudes of the amplitudes of the slow phases in a reaction assuming the sum of the two phases equals 100%. The amplitudes were obtained from the fits of the kinetic data using eq 2. [d] Only a single phase was observed in these kinetics monitored by scattering which has a magnitude somewhat near the value for the observed slower rate (k_{2obs}) monitored by fluorescence. [e] These experiments were carried out to kinetically confirm the results reported (from gel analysis) by Bochkareva et al. (*28*). The reactions were monitored by light scattering (see Materials and Methods) and included 10 mM Mg^{2+} and 1 mM 4,4′-DPDS in the presence or absence of 2 mM AMP-PNP. Other conditions are described in the legend of Figure 3.

in Figure 6. There is a clear indication that the level of monomer formation increased over time, going to near completion at ~60 min. This is demonstrated by overlaying the normalized gel densities [Figure 7 (●)] on a normalized kinetics profile monitored by fluorescence [Figure 7 (○)]. This shows that the fluorescence increase and extent of monomer formation are correlated, even though the experiments are very different.

Effect of Mg^{2+}, KCl, and Adenine Nucleotides. The effects of added Mg^{2+} and adenine nucleotides in the absence or presence of each other, and of KCl on the dissociation rate of GroEL by its reaction with 4,4′-DPDS, were investigated. The results are summarized in Table 1.

In a previous study, Bochkareva et al. (*28*) reported that AMP-PNP was able to promote the disassembly of GroEL by 4,4′-DPDS. As seen from the results presented here (Table 1), it is evident that although the observed kinetics were affected to different extents, all of these lead to the formation of monomers at the end of the reaction. This is evidenced by identical intensities at the plateau of kinetic traces for the series of reactions followed by a specific technique (fluorescence or scattering). All the kinetics monitored by fluorescence are clearly biphasic, except the case where only AMP was used. On the contrary, all the kinetics monitored by scattering were monophasic except when ADP-Mg^{2+} (with or without bis-ANS), AMP-PNP-Mg^{2+}, and ATPγS-Mg^{2+} were present in the reaction solution.

KCl alone had no effect when its concentration was varied from 0.001 to 0.3 M. The value of k_{obs} at 0.12 M is shown in Table 1 for the sake of comparison with other effects. The observed rate of dissociation of the GroEL 14mer increased ~1.5 times when the concentration of buffer (NaH_2PO_4/Na_2HPO_4) was increased from 10 mM to 0.2 M while all other reaction conditions were identical. There is a faster rate (k_{1obs} in Table 1) with a magnitude of $\sim 1 \times 10^{-2}$ s^{-1} in the following reactions: no Mg^{2+} or nucleotides, ATP, ADP, AMP-PNP-Mg^{2+}, AMP-PNP, ATPγS, and ATP-Mg^{2+} (no bis-ANS). The presence of Mg^{2+} gives a rate (7.43×10^{-3} s^{-1}) slightly lower than these values. Therefore, we can say that the above nucleotides do not specifically destabilize the 7mer rings with respect to this process. The fastest observed rates in the cases of other nucleotides such as AMP and ATPγS-Mg^{2+} are on the order of $\leq 6.29-1.14 \times 10^{-3}$ s^{-1} and therefore provide intraring stabilization. The presence of a slower rate process (k_{2obs}) with at least 20−40% of the total amplitude of the kinetics monitored by fluorescence indicates the presence of an intermediate that binds bis-ANS at a rate different from that of the initial binding. Such slow processes are not clearly distinguished by the light scattering technique. This is probably due to an intermediate with a size for light scattering similar to that of the 14mer, but differing in hydrophobic exposure for bis-ANS binding. Characterization of this intermediate is beyond the scope of this investigation. The biphasic kinetics are in agreement with our recently reported investigation on bis-ANS binding to GroEL, which demonstrated the availability of two types of binding sites with a K_d of ~0.56 μM for ~1.7 tight binding

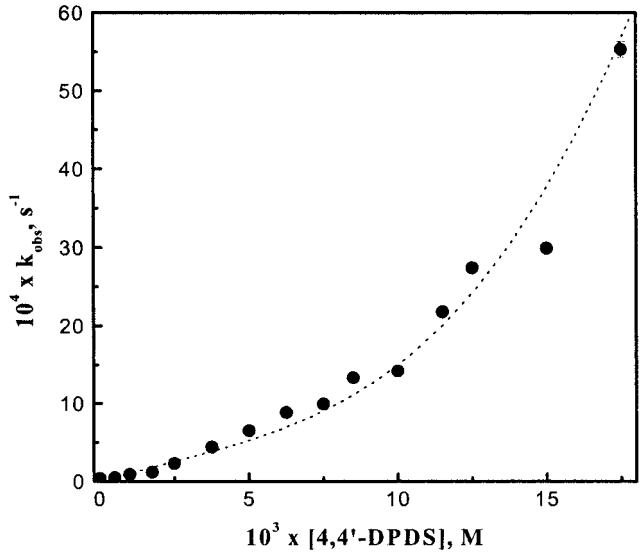

FIGURE 4: Dependence of the observed rates on 4,4′-DPDS concentration. Plot of the observed rates (k_{obs}) of dissociation of the GroEL 14mer by 4,4′-DPDS as a function of 4,4′-DPDS concentration. The k_{obs} values were obtained from fits to the kinetic data as described in Materials and Methods. The data presented in the plot are from reactions followed by scattering at 400 nm. The excitation and emission path lengths were 0.5 and 0.25 cm, respectively, and both slits were at 2 nm (band-pass). GroEL was incubated with bis-ANS for 1 h before the addition of 4,4′-DPDS. The reaction conditions were as follows: 0.83 μM GroEL 14mer, 5 μM bis-ANS, 10 mM Na_2HPO_4/NaH_2PO_4, pH 7.6, and 25 °C. The dashed line is an arbitrary line drawn to demonstrate the cooperativity between the observed rates and the increase in 4,4′-DPDS concentration.

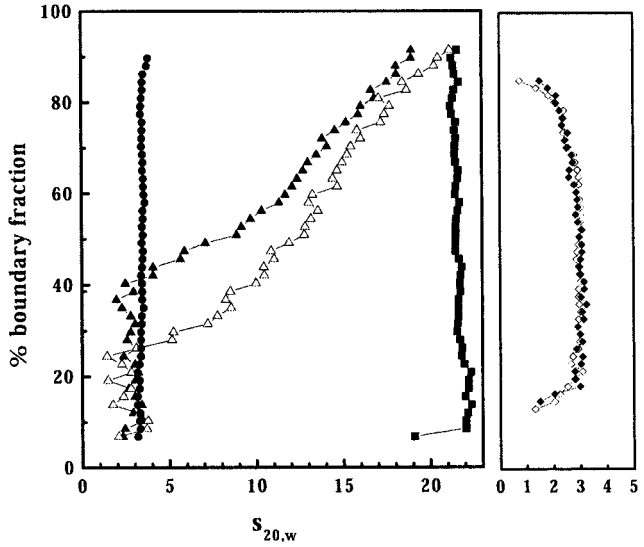

FIGURE 5: Sedimentation velocity data for the GroEL 14mer and monomers. Data for the GroEL oligomer (left panel, ■), the GroEL monomer formed by high pressure (left panel, ●), the GroEL monomer formed by the 4,4′-DPDS reaction after isolation for 2 h (left panel, ▲) and 4 h (left panel, △), and the GroEL monomers formed by the 4,4′-DPDS reaction after its isolation in buffer containing 1:1 4,4′-DPDS to cysteine residues for 2 h (right panel, ◆) and 6 h (right panel, ◇). All reactions were carried out in 10 mM sodium phosphate buffer at pH 7.6 and 25 °C.

sites and a K_d of ~10.57 μM for ~8.5 loose binding sites (*42*).

It is important to mention that the effects of AMP-PNP in the presence of Mg^{2+} and KCl shown in Figure 3 were studied using 1 mM rather than 5 mM 4,4′-DPDS that was

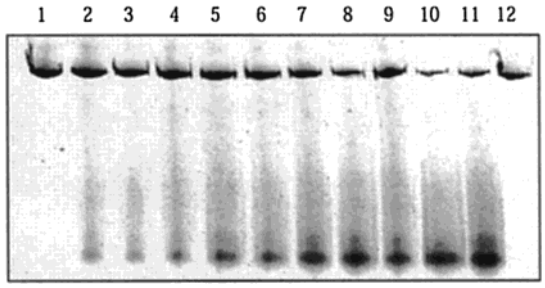

FIGURE 6: Monomer formation as a function of time. Discontinuous native gel (5%) of the GroEL 14mer and monomers, stained with Coomassie Blue G. All reactions were carried out in 10 mM sodium phosphate buffer (pH 7.6) and included 0.83 μM GroEL 14mer at 25 °C. Lane 1 is GroEL in an equivalent amount of ethanol as stock 4,4′-DPDS at the time the reaction was begun (0 min). Lanes 2−11 are GroEL reacted with 5 mM 4,4′-DPDS at 0, 5, 10, 15, 20, 25, 30, 40, 50, and 60 min. Lane 12 is GroEL in an equivalent amount of ethanol as stock 4,4′-DPDS at 60 min to demonstrate that the presence of ethanol is not causing monomerization.

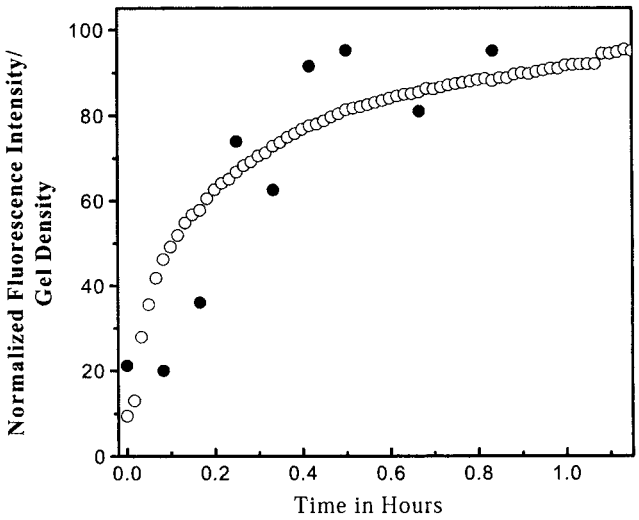

FIGURE 7: Comparison of the kinetics of monomer formation assessed by fluorescence and gel electrophoresis. The gel densities of GroEL monomers formed by the reaction of GroEL with 4,4′-DPDS are overlaid with the kinetics of an identical reaction followed by fluorescence. The gel densities are from the native gel shown in Figure 6. Kinetics were monitored by exciting the sample at 395 nm and recording the emission at 495 nm. The reaction conditions were as follows: 0.83 μM GroEL 14mer, 5 μM bis-ANS, 5.0 mM 4,4′-DPDS, 10 mM Na_2HPO_4/NaH_2PO_4, pH 7.6, and 25 °C. The excitation and emission path lengths were 0.5 and 0.25 cm, respectively, and both slits were at 2 nm (band-pass).

used in most of the experiments relevant to this investigation. Therefore, the last two entries in Table 1 are not to be confused with the rest of the results presented in the same table. These two experiments were carried out to kinetically confirm the effect of Mg^{2+}, AMP-PNP, and KCl when added together with those from the gel analysis of monomer formation reported by Bochkareva et al. (*28*). Their results show ~25% monomers in the absence of AMP-PNP and ~95% monomers in its presence after reaction for 90 min. In our study, in the absence of AMP-PNP, the kinetics were biphasic with a k_{1obs} of $(1.70 \pm 0.04) \times 10^{-4}$ s^{-1} and a k_{2obs} of $(6.00 \pm 0.05) \times 10^{-5}$ s^{-1} (trace A, Figure 3), whereas in the presence of AMP-PNP (2 mM), they were monophasic with a k_{obs} of $(2.10 \pm 0.01) \times 10^{-4}$ s^{-1} (trace B, Figure 3). The nature of the intermediate that accumulated during the reaction in the absence of AMP-PNP is beyond the scope of

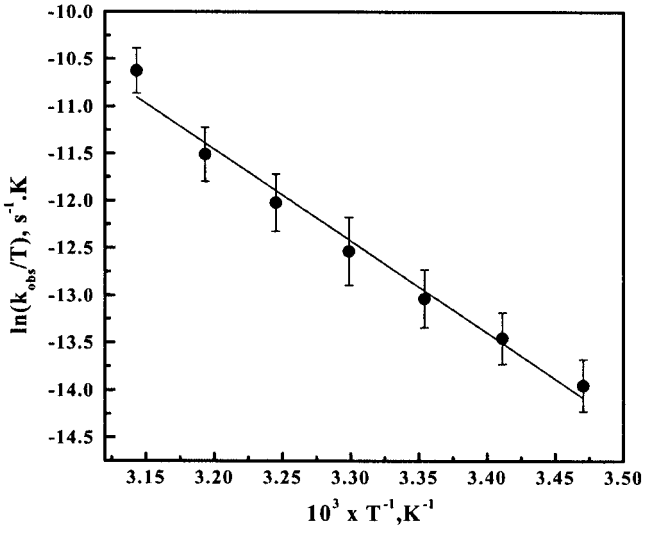

FIGURE 8: Temperature dependence of GroEL dissociation by 4,4′-DPDS. Eyring plot of $\ln(k_{obs}/T)$ vs T^{-1} showing the dependence of the rate of dissociation of the GroEL 14mer by the reaction with 4,4′-DPDS as a function of temperature. Thermodynamic parameters were calculated as described in Materials and Methods. All the kinetics were followed by scattering monitored at 400 nm. The excitation and emission path lengths were 0.5 and 0.25 cm, respectively, and both slits were at 2 nm (band-pass). GroEL was incubated with bis-ANS for 1 h before the addition of 4,4′-DPDS. The reaction conditions were as follows: 0.83 μM GroEL 14mer, 5 μM bis-ANS, 10 mM Na_2HPO_4/NaH_2PO_4, and pH 7.6.

our study. We have varied the AMP-PNP concentration from 1 to 10 mM in the absence of Mg^{2+} or KCl and observed a linear increase in the k_{obs} values (results not shown).

Temperature Dependence of the 4,4′-DPDS Reaction. The effect of temperature on the dissociation of the GroEL 14mer by the reaction of 4,4′-DPDS was studied in the range of 15−45 °C. The k_{obs} values from the temperature dependence of the reaction monitored by light scattering studies were used for this purpose, because these reactions were monophasic (Figure 2C) and follow the dissociation of the oligomer. The observed rates of dissociation of GroEL in the absence of 4,4′-DPDS in this temperature range were very small. For example, while the reaction at 45 °C was over (10 half-lives) in ~10 min, the self-dissociation (no 4,4′-DPDS) had proceeded to only 1−2% of the total amplitude (intensity) expected for the complete dissociation. Reactions at temperatures higher than 45 °C were not carried out to avoid errors in the reaction such as contributions from self-dissociation and pH variations. A plot of $\ln(k_{obs}/T)$ versus $1/T$ is shown in Figure 8. Thermodynamic parameters were evaluated from the slope and intercept of the linear plot as described in Materials and Methods. The computed free energy of activation ($\Delta G^{\ddagger}$) was 19.3 ± 1.2 kcal mol^{-1}; the enthalpy of activation ($\Delta H^{\ddagger}$) and the entropy of activation ($\Delta S^{\ddagger}$) were 19.3 ± 1.2 kcal mol^{-1} and −8.2 ± 3.9 cal mol^{-1} K^{-1}, respectively.

DISCUSSION

The GroEL 14mer can be dissociated into monomers by several methods such as by reaction with fluorescein-5-maleimide (*27*), producing the K4E mutation (*43*), by treatment with low concentrations of urea or guanidine hydrochloride (*30*), and by the application of high hydrostatic pressure (*26, 31*). Recently, Bochkareva et al. (*28*) demonstrated a very simple method by which GroEL monomers can be conveniently produced by reacting the 14mer with the sulfhydryl-modifying agent 4,4′-DPDS. Using this reaction with mutants of GroEL, they have shown that addition of AMP-PNP induces conformational changes in a segment containing Cys458 covering the nucleotide-binding pocket (*2*), which leads to the dissociation of the 14mer. Our report presents a systematic study of the kinetics of this reaction and the effect of functional ligands such as Mg^{2+} and nucleotides on the rates of dissociation.

The levels of exposure of hydrophobic surfaces upon monomerization by urea and guanidine hydrochloride (*9, 30*) and by high hydrostatic pressure (*26*) can be found in the literature. The monomers formed at high urea concentrations (4−8 M) were unfolded and do not reassociate back to the oligomer upon removal of urea except under conditions requiring 10 mM Mg^{2+}, 5 mM ATP, and 0.4 M $(NH_4)_2SO_4$ (*44*). In the high-pressure studies on GroEL dissociation, the bis-ANS fluorescence increases with the progress of dissociation ($p_{1/2}$ = 1.75 kbar; $t_{1/2}$ = 11.4 min), and upon depressurization, there was a slow decrease in fluorescence (*26*). These monomers were shown to reassociate very slowly (*26*). In our investigation, we have demonstrated that the hydrophobic exposure in 4,4′-DPDS-induced dissociation of GroEL probed by bis-ANS fluorescence follows the formation of monomers (see the Results and Figure 7).

From fluorescence and scattering studies, we demonstrated that the monomer formation is kinetically controlled and proceeds to completion. At very low concentrations of 4,4′-DPDS (<1 mM), the dissociation kinetics monitored by light scattering were also biphasic. The initial phase is most likely a lag phase in the reaction. In the series of experiments where the concentration of 4,4′-DPDS was varied, there is good evidence that the lag phase becomes progressively shorter, eventually leading to an apparent monophasic reaction (Figure 2C). The formation of an intermediate with a change in the conformational state, which dissociates slowly to the monomers, is most likely. The rate of dissociation increases with the increase in the concentration of 4,4′-DPDS and is cooperative (Figure 4), which suggests that the 7mer rings of the 14mer are progressively destabilized by increases in the 4,4′-DPDS concentration. The purified monomers formed at the end of the reaction and in the presence of 4,4′-DPDS showed a single component, similar to that of the monomers generated by pressure dissociation (Figure 5). The formation of monomers was correlated with the exposure of hydrophobic sites, which is demonstrated by the agreement of data from density measurements of the bands on native gels (Figure 6) with the kinetic trace monitored by fluorescence (Figure 7).

Since the dissociation process monitored by light scattering follows the 14mer to the dissociated monomers, any observed kinetics must be attributed to the decrease in its size. From the dependence of the rate on the 4,4′-DPDS concentration, it is reasonable to state that the process is cooperative. We varied the concentrations of 4,4′-DPDS to a maximum of 17.5 mM and found that the observed rate did not reach a plateau (Figure 4). Beyond 17.5 mM, there was visible precipitation of the protein. The dependence could also be due to a change in the rate-determining process of dissociation. However, if the rate-determining process follows the formation of disulfides by 4,4′-DPDS and the three individual

cysteines present in each subunit of the GroEL 14mer, then the situation becomes more complicated. Therefore, the most plausible explanation is that the initial modification of Cys458 destabilizes the oligomer, which has a conformation different from that of the original GroEL. In this altered conformation, the other cysteines (Cys519 and Cys138) are exposed for either internal disulfide exchange or reaction with 4,4′-DPDS. It is interesting to note that from double-mutant cycle analysis, Horvitz et al. (*45*) have reported the possibility of a long-range inter-residue interaction between Cys138 and Cys519. Also, chemical modification of the Cys138 residue by *N*-ethylmaleimide has been shown to affect the structure and function of GroEL (*46*). It is possible that 4,4′-DPDS used in our investigation might modify this residue during the reaction and enhance the dissociation of the GroEL 14mer. All these factors lead to a complicated dissociation process and are reflected in the concentration dependence of the observed rates as seen in Figure 4. The temperature dependence of the 4,4′-DPDS reaction is most probably coupled with the temperature dependence of the dissociation rate. In the absence of this reagent, no detectable self-dissociation of GroEL occurs at any kinetically significant rate; therefore, it is not possible to isolate the processes. The complexity of isolating individual rates for the 4,4′-DPDS reaction with the cysteines in GroEL can be appreciated in earlier work (*47*, *48*).

The effects of Mg^{2+} and nucleotides on the observed rates shown in Table 1 are difficult to group in magnitude order. Increasing the ionic strength by adding only KCl (0.001−0.3 M) did not have any effect on the rates. When the process was monitored by fluorescence, most of the reactions were biphasic. In contrast, most of the reactions are apparently monophasic when monitored by scattering. The only exceptions are that with AMP the kinetics appear to be monophasic when detected by fluorescence, whereas the scattering-monitored kinetics with ADP-Mg^{2+} (with or without bis-ANS), AMP-PNP-Mg^{2+}, or ATPγS-Mg^{2+} were biphasic. In an earlier investigation, we demonstrated that GroEL presents two types of bis-ANS binding sites (*42*). It is possible that the biphasic reactions in the presence of some of the nucleotides monitor either a single or mixture of transient species that are somewhat smaller than the 14mer, which further dissociate to the monomers in a slower process. It is also important to note that the slower processes have significant amplitudes, usually 10−40% of the total, and cannot be ignored. It is interesting to note that the presence of Mg^{2+} in the reaction mixture provided only a slight stabilization of the 14mer. This is in contrast to the observation from the high-pressure dissociation (*31*), where the presence of an identical amount of Mg^{2+} imparted dramatic stability against the dissociation of GroEL into monomers. The stabilization by Mg^{2+} to dissociation by pressure is an effect related to creation of "free volumes", solvent electrostriction, and solvation of nonpolar groups at boundaries of contact between the oligomer and monomer, which have been discussed in a recent publication (*31*). The minor effect of Mg^{2+} on the 4,4′-DPDS-induced dissociation suggests that the modification of Cys458 is able to destabilize the intraring cooperativity much more than the stabilization provided by the binding of Mg^{2+}. Since stability is a function of the rates in both the forward and reverse directions, the interpretation of stability and stabilization in this study is limited to the transition state relative to the native state.

The free energy of activation ($\Delta G^{\ddagger}$), enthalpy of activation ($\Delta H^{\ddagger}$), and entropy of activation ($\Delta S^{\ddagger}$) were 19.3 ± 1.2 kcal mol^{-1}, 19.3 ± 1.2 kcal mol^{-1}, and −8.2 ± 3.9 cal mol^{-1} K^{-1}, respectively (see the Results). The identical values of $\Delta G^{\ddagger}$ and $\Delta H^{\ddagger}$ within experimental error indicate that the computed value for $\Delta S^{\ddagger}$ is close to zero within experimental and computational errors. In conclusion, the major contribution to the kinetic barrier is from the enthalpy of activation with only a small contribution from the entropy of activation. According to the transition state theory, the enthalpy of activation is usually considered to be a measure of the energy barrier that must be overcome by the reacting or dissociating molecule to reach the products (*39*, *40*, *49*, *50*) and is always positive. A detailed discussion of the relevance of the transition state theory as applied to folding and catalysis by proteins has been discussed in the literature (*49*, *50*). The entropy of activation is a measure of the number of molecules having the requisite amount of energy that can actually react (*49*) and is composed of the sum of translational, rotational, and internal entropies (*50*). The translational entropy is usually large (9 kcal deg^{-1} mol^{-1}) at 25 °C and increases in small amounts even when the mass of the molecule is increased by 10-fold (*50*). The rotational entropies for large organic molecules are ∼30 cal deg^{-1} mol^{-1}, whereas internal rotations contribute about 3−5 cal deg^{-1} mol^{-1} (*50*). In the study presented here, the contribution from entropy is very small, which is characteristic of unimolecular dissociations that do not have steric or orientation requirements (*49*).

ACKNOWLEDGMENT

We thank Virgil Schirf for his help in analyzing the XLA data. We also thank Jesse Ybarra for the isolation and purification of the GroEL 14mer.

REFERENCES

1. Braig, K., Otwinowski, Z., Hegde, R., Boisvert, D. C., Joachimiak, A., Horwich, A. L., and Sigler, P. B. (1994) *Nature 371*, 578−586.
2. Boisvert, D. C., Wang, J., Otwinowski, Z., Horwich, A. L., and Sigler, P. B. (1996) *Nat. Struct. Biol. 3*, 170−177.
3. Braig, K., Adams, P. D., and Brunger, A. T. (1995) *Nat. Struct. Biol. 2*, 1083−1094.
4. Xu, Z., Horwich, A. L., and Sigler, P. B. (1997) *Nature 388*, 741−750.
5. Landry, S. J., Zeilstra-Ryalls, J., Fayet, O., Georgopoulos, C., and Gierasch, L. M. (1993) *Nature 364*, 255−258.
6. Fenton, W. A., Kashi, Y., Furtak, K., and Horwich, A. L. (1994) *Nature 371*, 614−619.
7. Xu, Z., and Sigler, P. B. (1998) *J. Struct. Biol. 124*, 129−141.
8. Azem, A., Diamant, S., and Goloubinoff, P. (1994) *Biochemistry 33*, 6671−6675.
9. Langer, T., Pfeifer, G., Martin, J., Baumeister, W., and Hartl, F. U. (1992) *EMBO J. 11*, 4757−4765.
10. Buchner, J., Schmidt, M., Fuchs, M., Jaenicke, R., Rudolph, R., Schmid, F. X., and Kiefhaber, T. (1991) *Biochemistry 30*, 1586−1591.
11. Zahn, R., and Pluckthun, A. (1994) *J. Mol. Biol. 242*, 165−174.
12. Hunt, J. F., Weaver, A. J., Landry, S. J., Gierasch, L., and Deisenhofer, J. (1996) *Nature 379*, 37−45.
13. Goloubinoff, P., Christeller, J. T., Gatenby, A. A., and Lorimer, G. H. (1989) *Nature 342*, 884−889.
14. Laminet, A. A., Ziegelhoffer, T., Georgopoulos, C., and Pluckthun, A. (1990) *EMBO J. 9*, 2315−2319.

15. Martin, J., Langer, T., Boteva, R., Schramel, A., Horwich, A. L., and Hartl, F. U. (1991) *Nature 352*, 36−42.
16. Viitanen, P. V., Lubben, T. H., Reed, J., Goloubinoff, P., O'Keefe, D. P., and Lorimer, G. H. (1990) *Biochemistry 29*, 5665−5671.
17. Brazil, B. T., Ybarra, J., and Horowitz, P. M. (1998) *J. Biol. Chem. 273*, 3257−3263.
18. Roseman, A. M., Chen, S., White, H., Braig, K., and Saibil, H. R. (1996) *Cell 87*, 241−251.
19. Hammarstrom, P., Persson, M., Owenius, R., Lindgren, M., and Carlsson, U. (2000) *J. Biol. Chem. 275*, 22832−22838.
20. Todd, M. J., Viitanen, P. V., and Lorimer, G. H. (1994) *Science 265*, 659−666.
21. Yifrach, O., and Horovitz, A. (2000) *Proc. Natl. Acad. Sci. U.S.A. 97*, 1521−1524.
22. Lin, Z., Schwartz, F. P., and Eisenstein, E. (1995) *J. Biol. Chem. 270*, 1011−1014.
23. Mendoza, J. A., Demeler, B., and Horowitz, P. M. (1994) *J. Biol. Chem. 269*, 2447−2451.
24. Mendoza, J. A., and Horowitz, P. M. (1994) *J. Biol. Chem. 269*, 25963−25965.
25. Horovitz, A., Bochkareva, E. S., and Girshovich, A. S. (1993) *J. Biol. Chem. 268*, 9957−9959.
26. Gorovits, B., Raman, C. S., and Horowitz, P. M. (1995) *J. Biol. Chem. 270*, 2061−2066.
27. Jai, E., and Horowitz, P. M. (1999) *J. Protein Chem. 18*, 387−396.
28. Bochkareva, E., Safro, M., and Girshovich, A. (1999) *J. Biol. Chem. 274*, 20756−20758.
29. Gorovits, B. M., and Horowitz, P. M. (1995) *J. Biol. Chem. 270*, 28551−28556.
30. Horowitz, P. M., Hua, S., and Gibbons, D. L. (1995) *J. Biol. Chem. 270*, 1535−1542.
31. Panda, M., Ybarra, J., and Horowitz, P. M. (2001) *J. Biol. Chem. 276*, 6253−6259.
32. Staniforth, R. A., Cortes, A., Burston, S. G., Atkinson, T., Holbrook, J. J., and Clarke, A. R. (1994) *FEBS Lett. 344*, 129−135.
33. Miller, D. M., Kurzban, G. P., Mendoza, J. A., Chirgwin, J. M., Hardies, S. C., and Horowitz, P. M. (1992) *Biochim. Biophys. Acta 1121*, 286−292.
34. Gorovits, B. M., Seale, J. W., and Horowitz, P. M. (1995) *Biochemistry 34*, 13928−13933.
35. *Scion Image* (2000) Scion Corp., Frederick, MD.
36. van Holde, K. E., and Weischet, W. O. (1978) *Biopolymers 17*, 1387−1403.
37. Demeler, B. (1998) http://www.biochem.uthscsa.edu/UltraScan.
38. Sober, H. (1968) *The Handbook of Biochemistry and Molecular Biology*, Chemical Rubber Co., Cleveland, OH.
39. Glasstone, S., Laidler, K. J., and Eyring, H. (1941) *The Theory of Rate Processes*, pp 1−25, McGraw-Hill Book Company, New York.
40. Espenson, J. H. (1981) *Chemical Kinetics and Reaction Mechanisms*, pp 116−133, McGraw-Hill Book Company, New York.
41. Sandstrom, J. (1982) *Dynamic NMR Spectroscopy*, Chapter 7, pp 108−123, Academic Press, New York.
42. Smoot, A. L., Panda, M., Brazil, B. T., Buckle, A. M., Fersht, A. R., and Horowitz, P. M. (2001) *Biochemistry 40*, 4484−4492.
43. White, Z. W., Fisher, K. E., and Eisenstein, E. (1995) *J. Biol. Chem. 270*, 20404−20409.
44. Ybarra, J., and Horowitz, P. M. (1995) *J. Biol. Chem. 270*, 22113−22115.
45. Horovitz, A., Bochkareva, E. S., Yifrach, O., and Girshovich, A. S. (1994) *J. Mol. Biol. 238*, 133−138.
46. Martin, J. (1998) *J. Biol. Chem. 273*, 7351−7357.
47. Brocklehurst, K., and Little, G. (1972) *Biochem. J. 128*, 471−474.
48. Brocklehurst, K., and Little, G. (1973) *Biochem. J. 133*, 67−80.
49. Jencks, W. P. (1987) *Catalysis in Chemistry and Enzymology*, Chapter 11, pp 605−614, Dover Publications, Inc., New York.
50. Fersht, A. R. (1999) in *Structure and Mechanism in Protein Science*, pp 54−102, 540−572, W. H. Freeman and Company, New York.

BI010831X